

Novel Dual-Band 28/38 GHz MIMO Antennas for 5G Mobile Applications

Hala M. Marzouk¹, Mohamed I. Ahmed^{2, *}, and Abdelhamed A. Shaalan¹

Abstract—This paper introduces new compact microstrip line fed dual-band printed MIMO antennas resonating at 28 GHz and 38 GHz which are appropriate for 5G mobile communications. The first design in this work is a two-element conventional rectangular microstrip patch antenna with inset feed intended for 28 GHz and 38 GHz bands. The second design is symmetric dual-band two-element MIMO slotted-rectangular patches via microstrip inset fed lines. The dual-band response is attained from inverted I-shaped slots inserted in main patches. The third design is symmetric dual-band four-element MIMO antenna with inverted I-shaped slotted rectangular patches. A slot formed DGS is inserted in the partial rectangular ground plane. The substrate size is $55 \times 110 \text{ mm}^2$, while the introduced antennas have very modest planar configurations and inhabit an insignificant area which make them fit easier within handset devices for the forthcoming 5G mobile communications. Better return losses and larger bandwidths are realized. The MIMO antennas have low mutual coupling without using any added constructions. The antenna systems offer appropriate values of directivity, gain, and radiation efficiency with anticipated reflection and correlation coefficient characteristics which are seemly for 5G mobile applications. The antenna systems are fabricated by a photolithography process that uses optic-radiation to copy the mask on a silicon slab by the aid of photoresist layers and measured using Vector Network Analyzer ZVA 67 (measures up to 67 GHz frequency) with a port impedance of 50Ω .

1. INTRODUCTION

In the preceding few years, there has been notable progress in wireless mobile systems with sophisticated data rates. Multiple-Input-Multiple-Output (MIMO) tools with greater amount of data rates and virtuous radiated efficiencies are the significant defy in recent 4G and forthcoming 5G wireless mobile communication systems. By increasing the number of radiators (antenna elements) at both the transmitter and receiver sides, there is an excessive improvement in data rate and channel capacity [1]. Newly, millimeter-wave frequency bands have been dealt with and below concentrating by the research societies round the entire world that makes it likely robust candidates for the following generation mobile communication [2]. The frequency bands deliberated are 28 GHz, 38 GHz, 60 GHz, and 73 GHz for the following generation. Antennas are a strict elementary part in any wireless system scheme. The millimeter waves at upper frequencies suffer from atmospheric absorption and path loss. Design of a high gain antenna with compact size is a challenge and a promising technique [3]. Still, bandwidth augmentation and size subtraction are seemly dominant design attentions for the applied utilization of microstrip antennas owing to the progression of one of the characteristics, which usually terminates in degeneration of the other [4]. Usually, for new RF designs the antenna elements must have the possessions of low profile, low cost, dual or multiple band operations, modest planar design, and squeezed

Received 23 March 2019, Accepted 22 May 2019, Scheduled 10 June 2019

* Corresponding author: Mohamed I. Ahmed (miahmed@eri.sci.eg).

¹ Electronics and Communications Department, Zagazig University, Zagazig, Egypt. ² Microstrip Department, Electronics Research Institute, Giza, Egypt.

size. A lot of research attention has been concerned with multiband antenna systems operating in the millimeter-wave frequency bands and have been aggressively explored [5].

Numerous designs having multi-band methods are stated at this time that are adopted in the 5G millimeter wave bands. In [6], a circular microstrip antenna with an elliptically slot at 28 GHz and 45 GHz is introduced. In [7], a MIMO antenna with triple bands for UWB functions with characteristics of one band notching adjusted at 5 GHz to stoppage the WLAN frequency is reported. The design of a two-dimensional slot antenna working only at 28 GHz which contained 8 essential elements in a 2×4 shape was announced in [8]. Two slot antennas covering dual bands at 28 and 38 GHz with band irregular at 33 GHz was presented in [2]. A single band antenna with gain enhancement performances at 28 GHz was offered in [9]. The cellular hand set PCB with single band four elements of a microstrip antenna on a low-cost substrate of FR-4 at 28 GHz was used in [10]. Design of an eight-element microstrip antenna array for 28 and 38 GHz for the next 5G communications was introduced in [11]. A proximity coupling feed slotted patch antenna at 28 GHz and 38 GHz was presented in [12]. A four-element antenna array for 28 GHz, 37 GHz, 41 GHz, and 74 GHz bands was offered in [13]. A massive MIMO for 28/38 GHz antenna was presented [14]. In [15], the design of eight elements dual-band MIMO antennas for coming smartphones was offered. The antenna had a size of $7 \times 15.5 \text{ mm}^2$ for 3.3–3.6 GHz and 4.8–5.0 GHz at fifth-generation bands. The work in [16] introduced an antenna consisting of a radiator with triangular shaping taking exponentially declined edges. The monopole antenna had a condensed area of $10 \times 12 \text{ mm}^2$. A 2×2 MIMO antenna existed with an envelope correlation coefficient fewer than 0.001 by measurement. For the earliest time extending to our expertise, this article accommodates various approaches of millimeter-wave (mmWave) 5G antennas for cellular smartphones [17].

In this article, a condensed MIMO antenna operation at 5G millimeter wave 28/38 GHz frequency bands is introduced for mobile communications. All MIMO antennas are fabricated on an inexpensive Rogers 5880 substrate (lossy) with $h = 0.508 \text{ mm}$ and $\epsilon_r = 2.2$ and loss tangent $\tan\delta = 0.0009$ with dimensions of $w \times L = 55 \times 110 \text{ mm}^2$. The antenna length is chosen as $55 \times 110 \text{ mm}^2$ to be appropriate to be used as the mobile circuit board approximately similar to the dimensions of iPhone SE handset. The introduced antennas offer acceptable results of respectable matched impedance bandwidths, dual-band notch ability, and decent radiation patterns. Finally, the designs of two-port and four-port MIMO antennas achieve essential isolation superior to 27 dB without using any added constructions. The MIMO antennas can be simply appropriate into the higher and lower boundaries of modern handheld devices due to its squeezed size. The simulated results display that the three intended MIMO antennas have a dual-band purpose at 28/38 GHz that comprise forthcoming 5G exploitations. Table 1 compares the antenna performance parameters of the cited work with the introduced work in this article. The objective of our exploration is, therefore, to solve the low performance and design difficulty of 5G antennas. In this work, easy fabrications of microstrip antennas are recommended.

2. SYSTEM DESIGN

The system design is accomplished in three main stages: arising from different two elements antenna design, symmetric two elements MIMO antenna design, and four elements MIMO antenna design. Each antenna configuration is a planar design and would be one of the right choices to get a multi-resonance effect. The three system designs are low cost and low profile printed slotted antennas for millimeter wave 5G mobile communications [18]. The nominated size of the system circuit board in all three designs is $55 \text{ mm} \times 110 \text{ mm}$, which is practical for 5G smartphones. The antenna models are fabricated by a photolithography process that uses optic-radiation to copy the mask on a silicon slab by the aid of photoresist layers and measured using Vector Network Analyzer ZVA 67 (measures up to 67 GHz frequency) with a port impedance of 50Ω .

2.1. Different Two-Element Antenna Designs

In this section, the design of a two-element antenna is introduced. The antenna is studied and fabricated for broadband wireless access provision at two dissimilar operating frequencies for 5G mobile applications which are 28 GHz and 38 GHz. The geometry of the specified antenna is demonstrated in Fig. 1. It is fabricated on a $W \times L = 55 \times 110 \text{ mm}^2$ Rogers RT5880 substrate of 0.508 mm thickness, dielectric

Table 1. Comparison between various antenna performance parameters in the literature review and the introduced antennas in this article.

Reference cited paper	Operating frequency (GHz)	Reflection coefficient (dB)	Minimum isolation (dB)	Gain (dB _i)	Efficiency (%)	Antenna size (mm ³)	Substrate, ϵ_r
[2]	28 & 38	-35 & -45	-	5.63	93 & 94	5 × 5 × 0.127	Rogers 5880, 2.2
[6]	28 & 45	-40, -14	-	7.6 & 7.21	85.6 & 95.3	6 × 6 × 0.578	Rogers 5880, 2.2
[7]	3.08–3.96, 6.2–8.93 & 10–16	-16, -12 & -25	-16	5, 4 & 5	85, 80 & 79	50 × 30 × 1.6	FR-4, 4.4
[8]	28	-35	-	9	-	29.9 × 28.7 × 0.13	RO3003, 3
[9]	28	-33	-	5.9	-	5 × 11 × 0.254	Rogers 5880, 2.2
[10]	28	-21.44	-	11.2	-	31.677 × 7.07 × 0.5	FR-4, 4.4
[11]	28 & 38	-35 & -37	-16	15.6 & 10	-	16 × 16 × 0.8	FR-4, 4.4
[12]	28 & 38	-18 & -20	-	8.63 & 8.62	-	15 × 20 × 1.27	Ferro A6-M, 5.9
[13]	28, 37, 41 & 74	-22, -37, -10 & -19	-	4, 5.2, 7.2 & 12.5	-	26.6 × 3.2505 × 1.6	FR-4, 4.4
[14]	28 & 38	-17 & -28	-30	12.07 & 13.46	-	13 × 20 × 0.254	Rogers 5880, 2.2
Our first design	27.946 & 37.83	-27.84 & -18.35	-30	7.18 & 9.24	91.24 & 89.63	55 × 110 × 0.508	Rogers 5880, 2.2
Our second design	28.044 & 37.928	-19.91 & -26.12	-27	7.88 & 9.49	89.74 & 88.59	55 × 110 × 0.508	Rogers 5880, 2.2
Our third design	28.044 & 38.04	-21.57 & -24.59	-26	7.95 & 8.27	89.89 & 88.25	55 × 110 × 0.508	Rogers 5880, 2.2

constant $\epsilon_r = 2.2$, and loss tangent $\tan \delta = 0.0009$. The top and bottom patches printed on the substrate are the two radiating configurations and the ground plane which are formed of copper material. Initially, the dimensions of essential radiating patches are calculated in accordance with the chosen resonant frequency. There are two dissimilar operating frequencies for dual-band operation. By means of antenna theory [19], the 28 GHz antenna acquires patch size of $W_{28} \times L_{28} = 3.44 \times 3.35 \text{ mm}^2$ with inset feed of $g \times d_1 = 0.2 \times 1.2 \text{ mm}^2$ as in Fig. 1(c). Fig. 1(d) illustrates the 38 GHz antenna that acquires patch size of $W_{38} \times L_{38} = 3.3 \times 2.4 \text{ mm}^2$ with inset feed of $g \times d_2 = 0.2 \times 0.7 \text{ mm}^2$. The patches are fed by a microstrip transmission line to motivate the appropriate set of dimensions $W_F \times L_F = 1.55 \times 2.61 \text{ mm}^2$ to attain

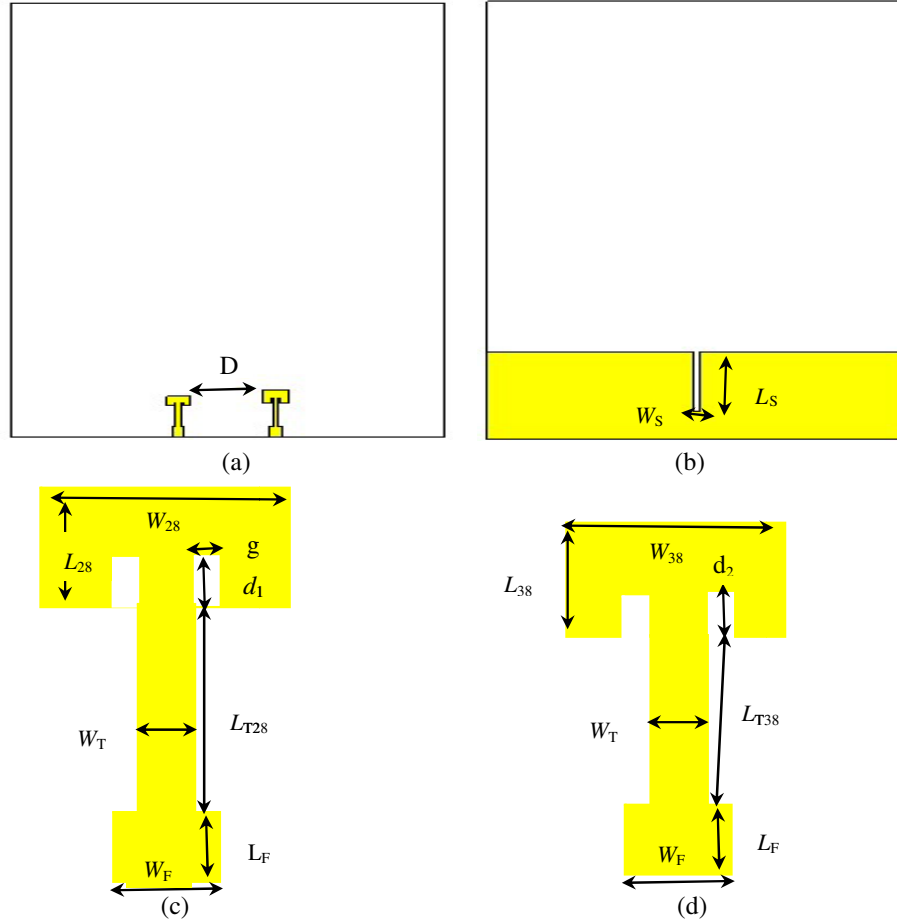


Figure 1. Antenna Geometry. (a) Top view, (b) back view, (c) 28 GHz antenna and (d) 38 GHz antenna.

50 Ω input impedance matching. The feeding is not directly constructed on the patch edges but by using multiple quarter wavelength transformers of 75 Ω with dimensions $W_T \times L_{T28} = 0.8 \times (3 \times 1.98)$ mm² and $W_T \times L_{T38} = 0.8 \times (3 \times 1.74)$ mm² for 28 GHz and 38 GHz, respectively. The back view is illustrated in Fig. 1(b) which is the ground plane of dimensions $W \times L_g = 55 \times 22$ mm² with a slot dimension of $W_S \times L_S = 1 \times 15.07$ mm². An extended rectangular strip is imprinted from the ground plane between the two antennas to additional reduction in the mutual coupling and increment in the impedance bandwidth [20]. The focal principle for multi-port design is mutual coupling, which mostly rises due to the smaller distance between the two antennas, by expanding the distance between the two antenna elements, and the mutual coupling can be diminished. The parting between the two edges of the patch antennas is $D = 10.13$ mm which is about λ to evade grating lobes. The width and length of the inset feed have an expressive influence on the resonant frequencies and return loss levels, so the greatest satisfactory results should be achieved and established on optimization and numerous parametric cases. On the back side of the substrate, a slot is engraved on the ground to upgrade impedance matching and isolation. The concluding optimized parameters are listed in Table 2.

2.2. Experimental Results

The antenna performance is measured by Vector Network Analyzer ZVA 67 (measures up to 67 GHz frequency) with a port impedance of 50 Ω . The comprehensive integrated systems resonate at 28 GHz and 38 GHz. The array is auxiliary analysed and fabricated for the following parameters.

Table 2. Total dimensions of the introduced antenna.

Parameter	Dimension (mm)	Parameter	Dimension (mm)
W	55	W_T	0.8
L	115	L_{t28}	5.94
W_{28}	3.44	L_{t38}	5.22
L_{28}	3.35	g	0.2
W_{38}	3.3	d_1	1.2
L_{38}	2.4	d_2	0.7
W_F	1.55	h	0.508
L_F	2.61	L_g	22
W_S	1	L_s	15.07
D	10.13		

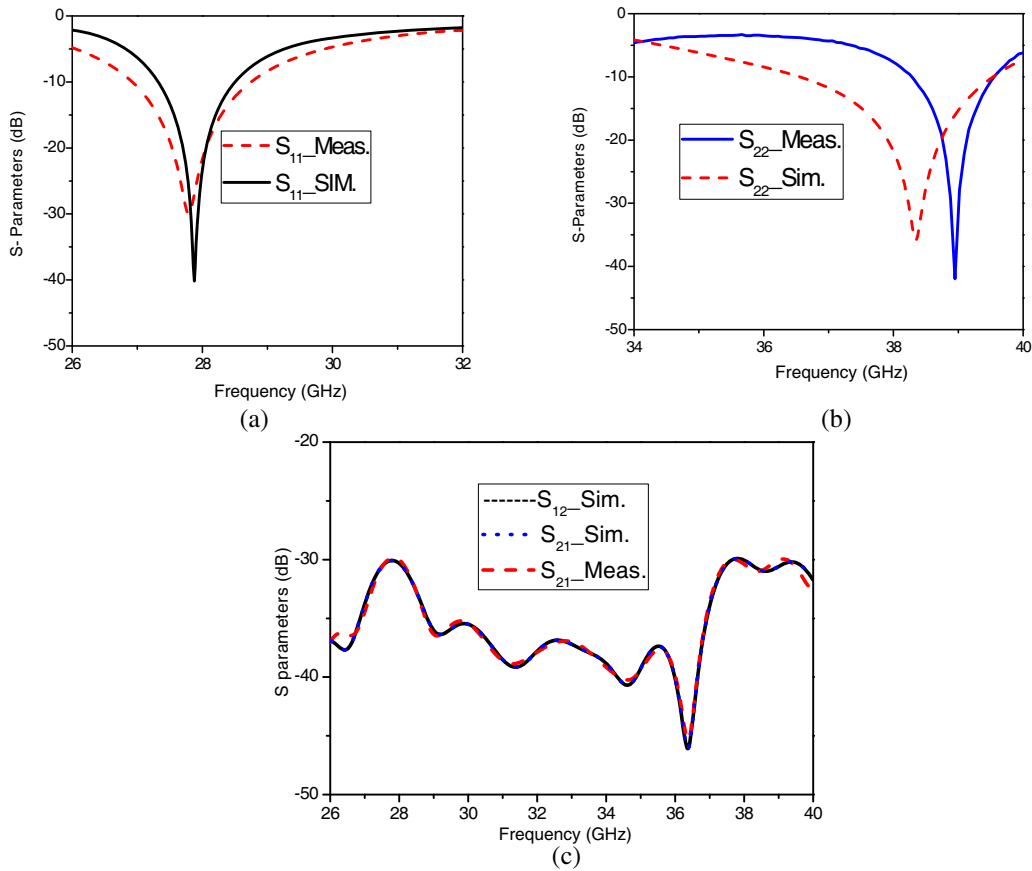


Figure 2. Reflection coefficients for two element antenna. (a) $|S_{11}|$, (b) $|S_{22}|$ and (c) transmission coefficients.

2.2.1. Return Loss and Mutual Coupling

Figs. 2(a), 2(b) demonstrate the $|S_{11}|$ and $|S_{22}|$ plots after simulation and fabrication. We can perceive $|S_{11}|$ and $|S_{22}| < -10$ dB for the 28 GHz and 38 GHz mm-Wave band frequencies. As a result, both antennas befit the wanted necessities of the return loss. The two elements provide 27.946 GHz and

37.83 GHz frequencies from simulation, and the measured two-element design provides 28.3 GHz and 38.9 GHz frequencies. All of these bands are subjected in 5G wireless communication. The plot in Fig. 2(c) illustrates the transmission coefficients for the two-port antenna system. We can perceive S_{21} and $S_{12} < -29$ dB for 28 GHz and 38 GHz mm-wave frequencies; therefore, the two antennas are independent of each other. and the mutual coupling value between the two antennas is very low. There is a respectable match between the results attained from simulation and measurement. Besides, there are no separate constructions of isolation used among antenna elements, and outstanding isolation is realized. The dissimilarity between the obtained results from simulation and measurement of reflection and transmission coefficients may be due to the tolerance in fabrication, loss tangent of the Rogers substrate, mismatching between the connector and antenna feeder, SMA connector loss, inadequate soldering of the SMA connector, and environmental effect.

2.2.2. Surface Current Distribution

To give a good vision on the operation of the introduced antenna, the surface current distributions are explored at the frequencies of 28 and 38 GHz using CST software as shown in Fig. 3. It is explicit that the surface current primarily focuses on the main patches at the resonant frequencies of 28 GHz and 38 GHz, respectively.

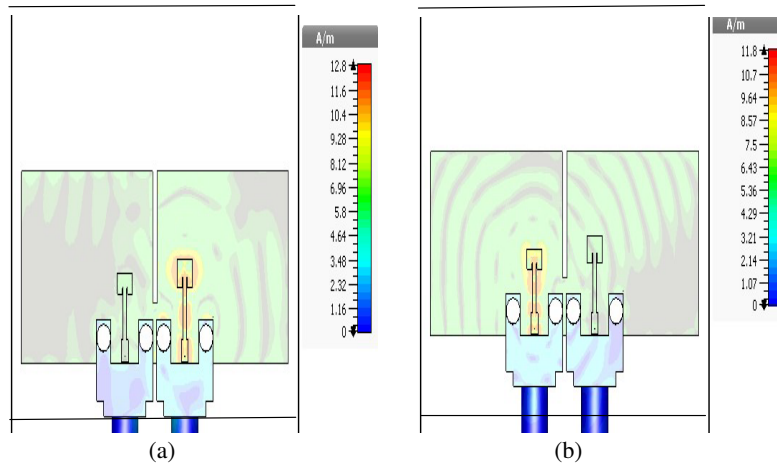


Figure 3. Current distributions of introduced different two element antenna at (a) 28 GHz and (b) 38 GHz.

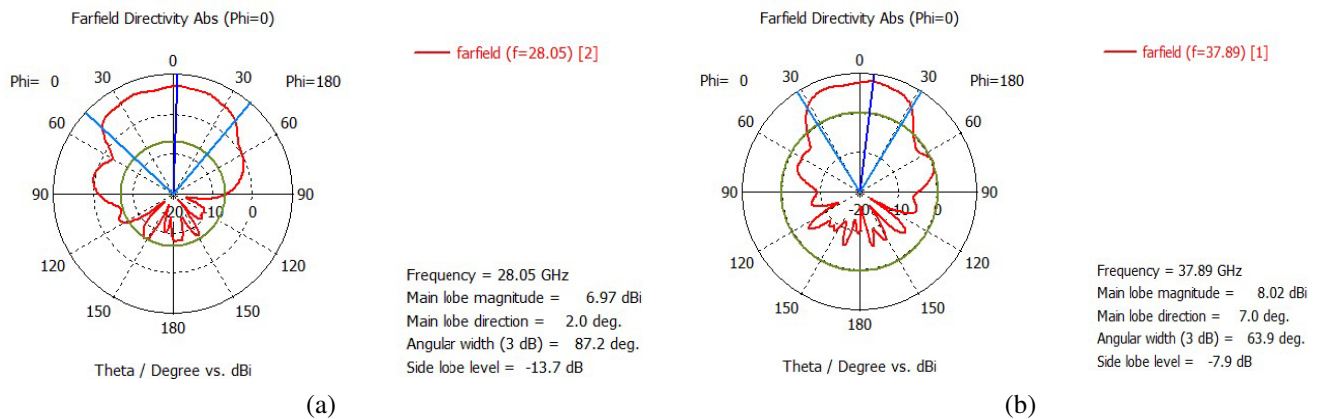


Figure 4. Farfield radiation pattern at (a) 28 GHz and (b) 38 GHz.

2.2.3. Gain and Radiation Pattern

The patterns of the radiated far-field of the antenna are presented in Fig. 4. The simulated directivity, gain, and efficiency of the mm-wave two-element antenna reach 7.581 dBi, 7.182 dBi, and 91.24% at 28 GHz and 9.716 dBi, 9.24 dBi and 89.63% at 38 GHz, respectively. The introduced antenna performs very well in the chosen frequency bands. The results gained from positioning two-element antenna in one design are better than that gained from single separated elements, and there is an enlargement in all antenna parameters.

Figure 5 illustrates photographs of the different two-element 5G antennas which are fabricated by a photolithography process that uses optic-radiation to copy the mask on a silicon slab by the aid of photo resist layers.

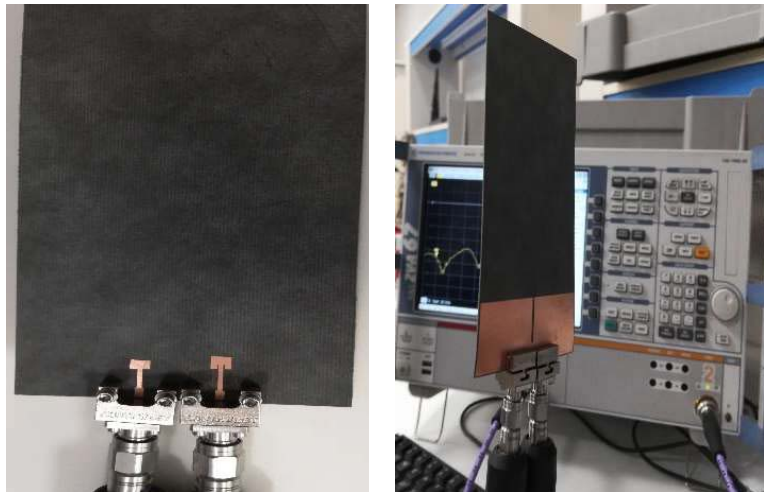


Figure 5. Photograph of introduced different two element 5G antenna.

3. SYMMETRIC TWO-ELEMENT MIMO ANTENNA DESIGN AND RESULTS

3.1. Antenna Design

In this subsection, a compact two-element dual-band slotted microstrip MIMO antenna for mobile communication applications is constructed and fabricated. The MIMO antenna is achieved by presenting two rectangular microstrip patch elements and cutting inverted I-shaped slots at the upper sides of the patches as revealed in Fig. 6. This antenna is designed on a lossy Rogers 5880 substrate with $h = 0.508$ mm, $\epsilon_r = 2.2$, and loss tangent $\tan \delta = 0.0009$ with size of $w \times L = 55 \times 110$ mm². The slots imprinted in the rectangular patches vary with altered sizes of cutting lengths. This variation leads to decent matching at the wanted frequencies. The slot dimensions are revealed in Fig. 6(c). The single antenna develops patch size of $W_P \times L_P = 4.59 \times 2.82$ mm² with inset feed of $g \times L_i = 0.2 \times 1.2$ mm². The two patch edges are separated by a distance of $D = 9.41$ mm (about 0.87λ) to evade mutual coupling and grating lobes. Hence, the two separated antennas in the introduced MIMO system are sufficient when being related to other systems. The ultimately adjusted parameters are listed in Table 3.

3.2. Experimental Results

3.2.1. Return Loss and Mutual Coupling

For the MIMO antenna composed of two elements, the -10 dB BWs realized at 28 GHz and 38 GHz are 1.0683 (27.58–28.649) GHz and 1.4306 (37.213–38.643) GHz, respectively. The simulated and measured reflection coefficients of the introduced antenna are displayed in Fig. 7(a). The measured and simulated data are in a respectable match with acceptable frequency discrepancies. Only S_{11} and S_{21} coefficients

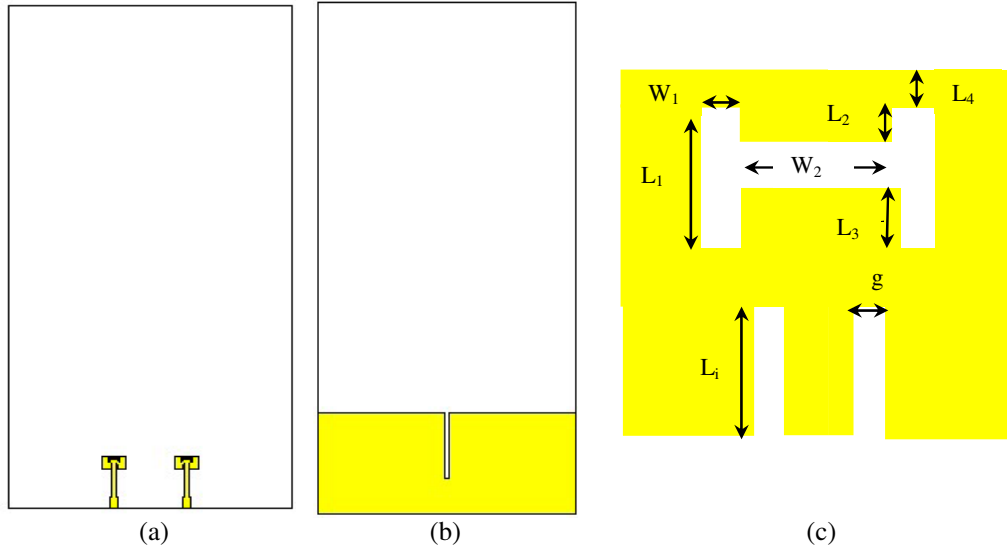


Figure 6. Two-element MIMO antenna. (a) Top view, (b) bottom view and (c) single element geometry.

Table 3. Total dimensions of introduced MIMO antenna.

Parameter	Dimension (mm)	Parameter	Dimension (mm)
W	55	W_T	0.8
L	110	L_t	5.94
W_P	4.59	h	0.508
L_P	2.82	g	0.2
W_F	1.55	L_i	1.2
L_f	2.61	D	9.41
W_S	1	L_g	22
L_s	14.35	L_3	0.4
L_1	1	W_1	1.6
L_2	0.2	W_2	0.3

are given, owing to the similarity of the two elements. It is remarkable that inter-element mutual coupling is decreased by separating the elements. The isolation is superior to -29.34 dB and -27.28 dB for the lower and higher frequencies, respectively.

3.2.2. Surface Current Distribution

Figure 8 demonstrates the surface current distributions at the frequencies of 28 and 38 GHz. It is obvious that the surface currents predominantly focus on the main patch at the resonant frequency of 28 GHz, in the “close to the inner area of the I-slots”. The current paths rise at the resonant frequency of 38 GHz due to the movement of the current around the slots.

3.2.3. Gain and Radiation Pattern

The obtained gain in this study is the optimal gain of a single patch microstrip slotted antenna. The antenna system offers maximum directivity, gain, and efficiency of 8.63 dBi, 7.882 dBi and 89.74% at 28 GHz and 10.021 dBi, 9.494 dBi and 88.59% at 38 GHz, respectively. The attained sidelobe levels are -8.3 dB at 28 GHz and -1.1 at 38 GHz as shown in Fig. 9.

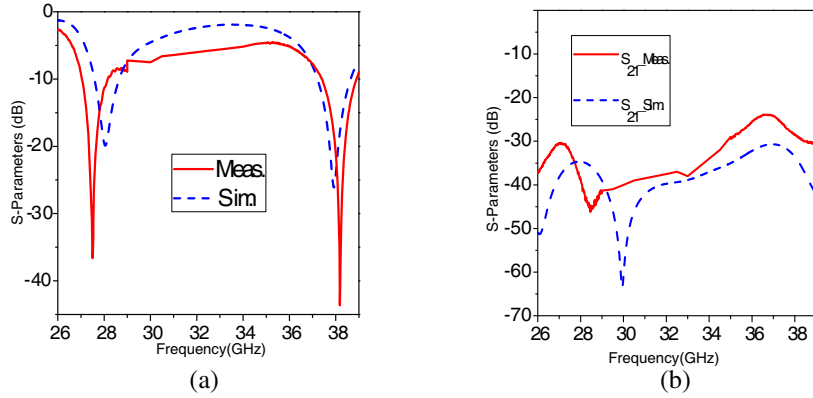


Figure 7. *S*-parameters of introduced two element MIMO antenna. (a) Reflection coefficient and (b) transmission coefficient.

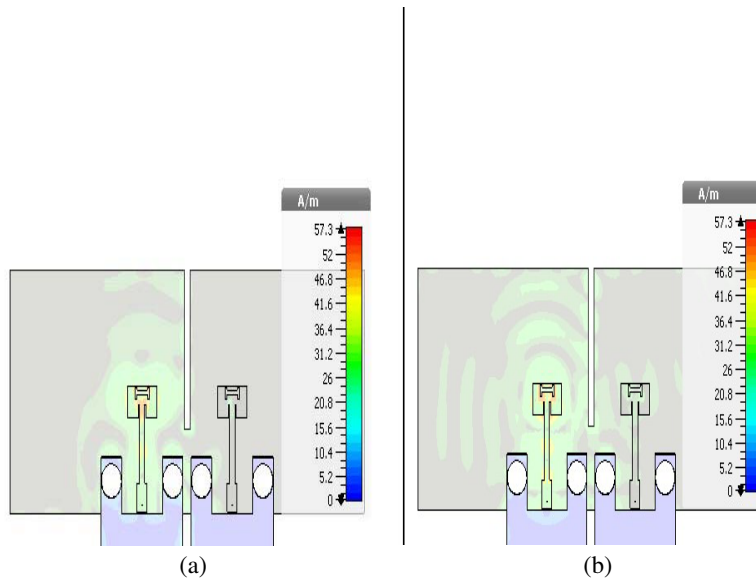


Figure 8. Current distributions of introduced two element MIMO antenna at (a) 28 GHz and (b) 38 GHz.

In the higher frequency band, the antenna gain is bigger. On the other hand, the radiation efficiency is reduced at the higher band. This may well be owing to the point that the directivity increases at the higher frequencies. The radiation efficiency η is the relation between gain g and directivity D , and while the directivity increases, the radiation efficiency decreases rendering to Eq. (1). The loss tangent $\tan \delta$ (happens due to the resistance in the dielectric) increases with frequency. This diminishes the radiation efficiency at higher frequencies but by the way of the directivity (which the radiation efficiency is not taken into account) increases for that specific frequency, and consequently the antenna gain at that frequency increases [21].

$$g = \eta x D \tag{1}$$

3.2.4. Correlation Coefficient

A significant factor for MIMO antenna characterization is the correlation coefficient (ρ). It is a measure of the isolation between numerous MIMO antenna channels and the correlation between signals received at similar sides of a wireless link. The envelop correlation coefficient (ECC) is used to estimate the diversity proficiency of multiple antenna systems by Eq. (2), in which small ECC value means greater isolation and large diversity gain. ρ should be smaller than 0.5 for decent MIMO process. This value

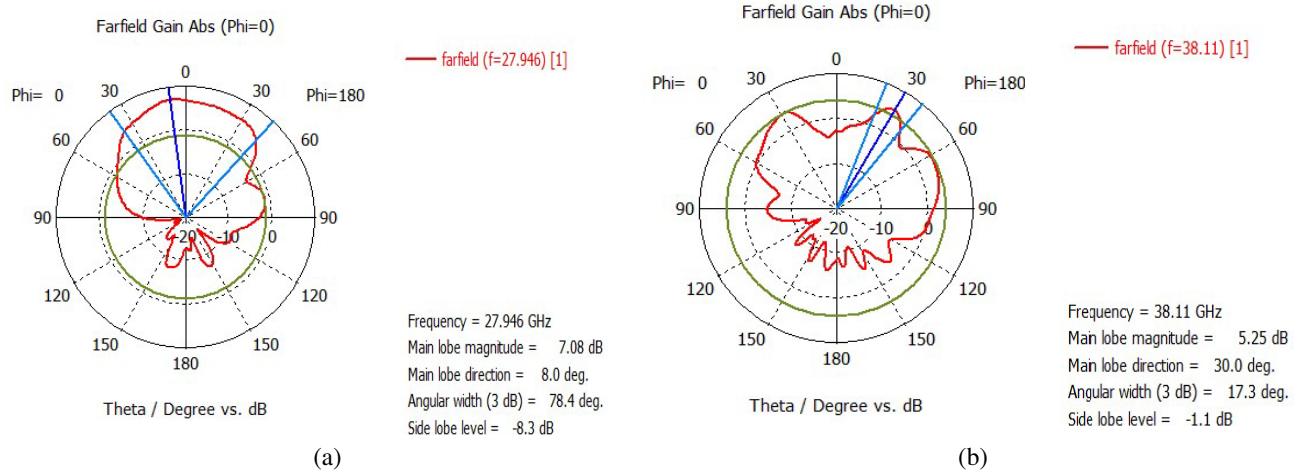


Figure 9. Simulated gain of introduced two element MIMO antenna.

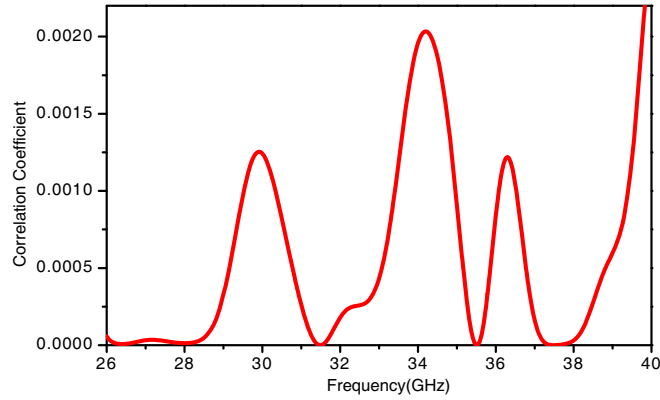


Figure 10. Envelope correlation coefficient of MIMO antenna.

is considered by the square root of the envelope correlation coefficient which can be calculated in a constant multipath situation using [22]. For the offered MIMO antenna system, ρ is calculated at the two frequencies 28 and 38 GHz, and the corresponding obtained values are 1.36×10^{-5} and 3.86×10^{-5} , respectively as publicized in Fig. 10. It is noticeable that the designed MIMO antenna system satisfies the requirement for good MIMO operation for 5G mobile applications.

$$ECC(\rho) = \frac{|S_{11} * S_{12} + S_{21} * S_{22}|^2}{(1 - |S_{11}^2| - |S_{21}|^2)(1 - |S_{22}|^2 - |S_{12}|^2)} \quad (2)$$

Figure 11 shows the fabricated two-element MIMO 5G antenna.

4. FOUR ELEMENTS MIMO ANTENNA DESIGN AND RESULTS

4.1. Antenna Design

In this subsection, the design of a four-element dual-band 28/38 GHz printed slotted microstrip antenna for the upcoming 5G mobile networks is introduced. By precisely employing two antennas of a similar variety at the lower verge and employing two antennas of a similar variety at the higher edge situated on the same $110 \times 55 \text{ mm}^2$ PCB of the mobile substrate, the four-element MIMO antenna is formed. The four-port MIMO antenna is considered as displayed in Fig. 12. The antennas in the array have similar dimensions as declared in Section 3.1.

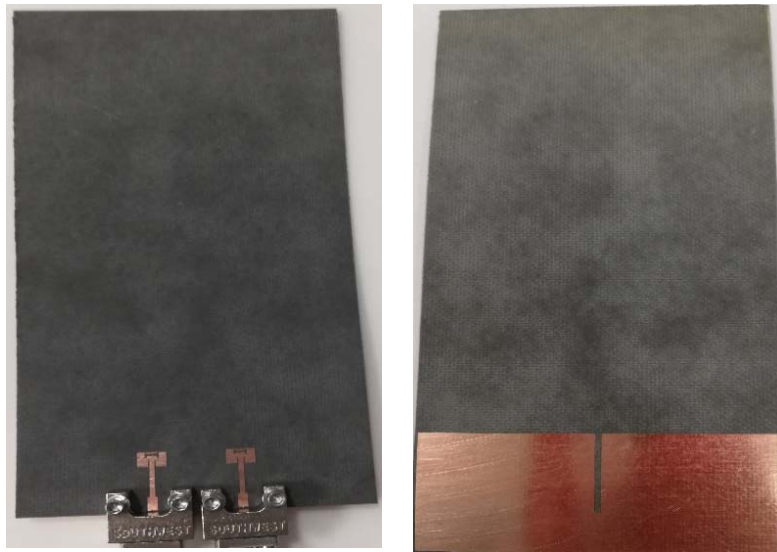


Figure 11. Photograph of introduced two-element MIMO 5G antenna.

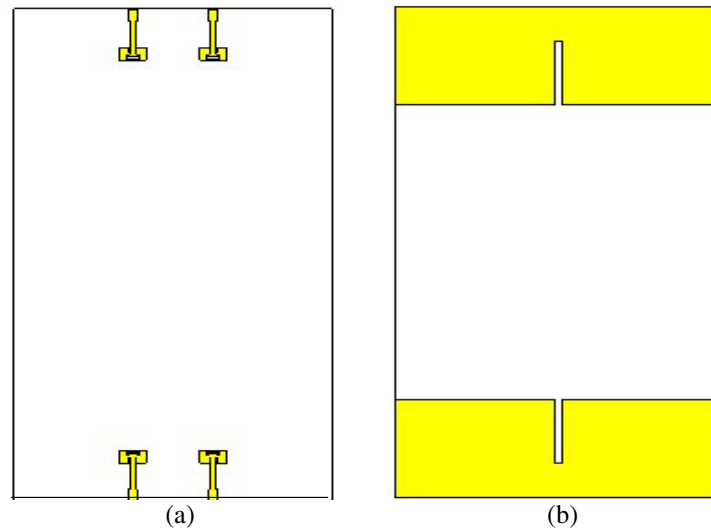


Figure 12. Four-element MIMO antenna. (a) Top view and (b) bottom view.

4.2. Experimental Results

4.2.1. Return Loss and Mutual Coupling

The reflection coefficients $|S_{11}|$ for the introduced four-element 5G MIMO antenna intended from simulation and measurement are illustrated in Fig. 13. It is obvious that the introduced MIMO antenna has moral matched impedances at the two wanted frequency bands of 28/38 GHz for $|S_{11}|$ smaller than -10 dB. Due to the similarity between the four elements, only S_{11} , S_{21} , S_{31} , and S_{41} coefficients are displayed in figures. The isolation is superior to -28.32 dB and -26.27 dB for the higher and lower frequency bands, respectively. It is distinguished that inter-element mutual coupling values are reduced from the two elements MIMO system introduced in this paper.

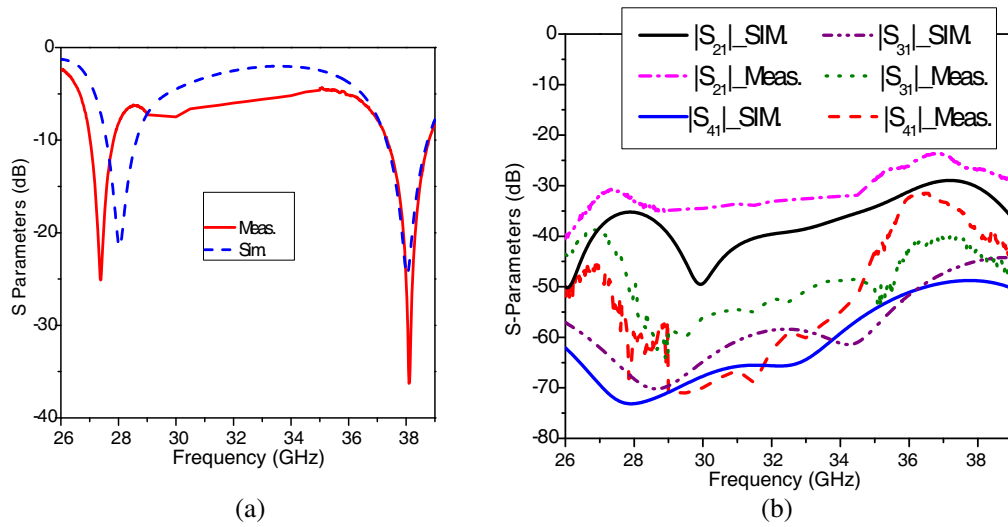


Figure 13. Four-element MIMO antenna. (a) Reflection coefficients and (b) transmission coefficients.

4.2.2. Surface Current Distribution

Figure 14 demonstrates the surface current distributions of the four-element MIMO antenna at frequencies of 28 and 38 GHz.

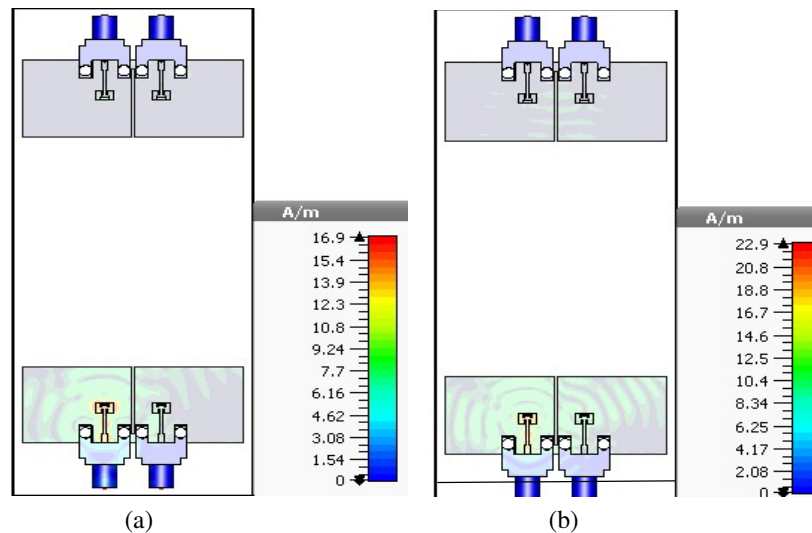


Figure 14. Current distributions of introduced four element MIMO antenna at (a) 28 GHz and (b) 38 GHz.

4.2.3. Gain and Radiation Pattern

The radiation pattern of the introduced four-element MIMO antenna outcomes from the simulation is obtained in Fig. 15. The antenna system shows available maximum and stable directivity, gain, and radiation efficiency of 8.409 dBi 7.946 dBi and 89.89% for the first band of 28 GHz and 8.808 dBi, 8.265 dBi and 88.25 % for the second band of 38 GHz, respectively. The attained sidelobe levels are -18.2 dB and -3.5 at 28 GHz, 38 GHz, respectively.

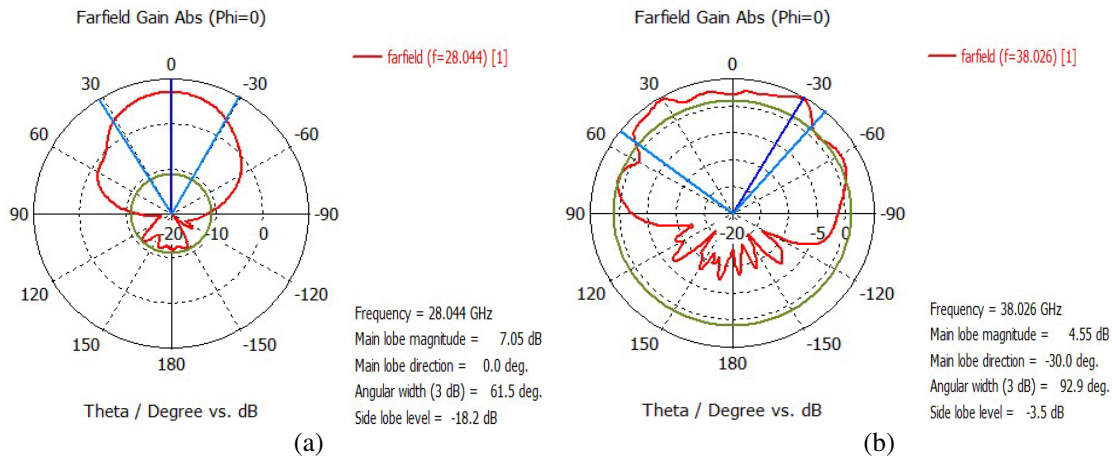


Figure 15. Simulated gain of introduced four element MIMO antenna for (a) 28 GHz and (b) 38 GHz.

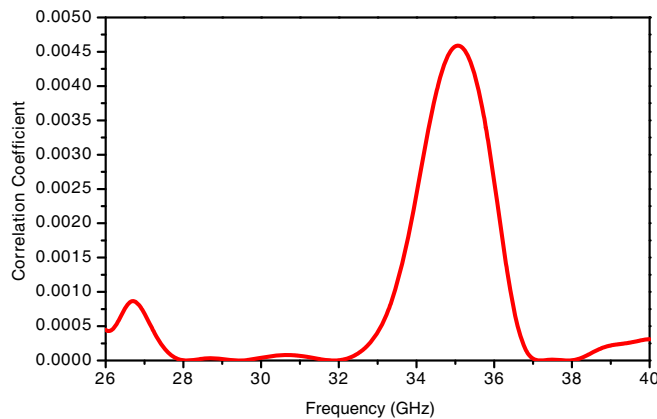


Figure 16. Envelope correlation coefficient of 4-element MIMO antenna.



Figure 17. Photograph of introduced four element MIMO 5G antenna.

4.2.4. Envelope Correlation Coefficient

For the introduced four-element MIMO antenna system, ρ is intended at the two frequencies 28 GHz and 38 GHz, and the equivalent gained values are 2.46×10^{-5} and 7.65×10^5 , respectively as exhibited in Fig. 16. It is noticeable that the considered MIMO antenna system gratifies the requirements for decent MIMO operation for 5G mobile applications. Fig. 17 displays the fabricated four-element MIMO

5G antenna.

Such designs are very smart to be combined in the upcoming mobile terminals for short-range 5G mobile communications. The simulated reflection and mutual coupling coefficients, gain, and envelope correlation coefficient values of the introduced two and four elements antennas at the two wanted frequencies are exposed in Table 4.

Table 4. Final parameters of the introduced antennas.

Antenna Design	Resonance Frequency (GHz)	Reflection Coefficient (dB)	Mutual Coupling (dB)	Gain (dBi)	Envelope Correlation Coefficient
Two Element Different Antennas	27.946	-27.84	-30.21	7.18	-
	37.83	-18.35	-29.91	9.24	-
Two Element Symmetric Antenna	28.044	-19.91	-29.34	7.88	1.36×10^{-5}
	37.928	-26.12	-27.28	9.49	3.86×10^{-5}
Four Element MIMO Antenna	28.044	-21.57	-28.32	7.95	2.46×10^{-5}
	38.04	-24.59	-26.27	8.27	7.65×10^{-5}

5. CONCLUSION

Novel compact microstrip line fed dual-band printed MIMO antennas for wireless mobile communication applications are presented. The introduced MIMO antennas are planned to be functioned at 28 GHz and 38 GHz which are appropriate for 5G mobile applications. The substrate size is $55 \times 110 \times 0.508 \text{ mm}^3$, while the introduced antennas have very modest planar constructions and occupy an insignificant area which makes them simpler to fit within handheld devices for the forthcoming 5G mobile communications. Better return losses and larger bandwidths are accomplished than some of the cited works as in [7, 12, 13]. The MIMO antennas have small mutual coupled values without using added constructions for isolation. The antenna systems offer moderate values of directivity, gain, and radiation efficiency with desirable reflection and correlation coefficients characteristics which are appropriate for next 5G communication applications.

REFERENCES

1. Babu, K. V. and B. Anuradha, "Design of multi-band minkowski MIMO antenna to reduce the mutual coupling," *Journal of King Saud University-Engineering Sciences*, 2018.
2. Ashraf, N., O. M. Haraz, M. M. M. Ali, M. A. Ashraf, and S. A. S. Alshebili, "Optimized broadband and dual-band printed slot antennas for future millimeter wave mobile communication," *AEU-International Journal of Electronics and Communications*, Vol. 70, 257–264, 2016.
3. Sulyman, A. I., A. T. Nassar, M. K. Samimi, G. R. MacCartney, T. S. Rappaport, and A. Alsanie, "Radio propagation path loss models for 5G cellular networks in the 28 GHz and 38 GHz millimeter-wave bands," *IEEE Communications Magazine*, Vol. 52, 78–86, 2014.
4. Islam, M. T., M. N. Shakib, and N. Misran, "Broadband EH shaped microstrip patch antenna for wireless systems," *Progress In Electromagnetics Research*, Vol. 98, 163–173, 2009.
5. Hong, W., Z. H. Jiang, C. Yu, J. Zhou, P. Chen, Z. Yu, et al., "Multibeam antenna technologies for 5G wireless communications," *IEEE Transactions on Antennas and Propagation*, Vol. 65, 6231–6249, 2017.
6. Khattak, M. I., A. Sohail, U. Khan, Z. Barki, and G. Witjaksono, "Elliptical slot circular patch antenna array with dual band behaviour for future 5G mobile communication networks," *Progress In Electromagnetics Research C*, Vol. 89, 133–147, 2019.

7. Kumar, A., A. Q. Ansari, B. K. Kanaujia, J. Kishor, and N. Tewari, "Design of triple-band MIMO antenna with one band-notched characteristic," *Progress In Electromagnetics Research C*, Vol. 86, 41–53, 2018.
8. Alreshaid, A. T., O. Hammi, M. S. Sharawi, and K. Sarabandi, "A compact millimeter-wave slot antenna array for 5G standards," *2015 IEEE 4th Asia-Pacific Conference on Antennas and Propagation (APCAP)*, 84–85, 2015.
9. Ali, M. M. M. and A.-R. Sebak, "Directive antennas for future 5G mobile wireless communications," *General Assembly and Scientific Symposium of the International Union of Radio Science (URSI GASS)*, 1–4, 2017.
10. Hegazy, M. B. E. M. E. A., "Design and analysis of 28 GHz rectangular microstrip patch array antenna," *WSEAS Transactions on Communications*, Vol. 17, 1–9, 2018.
11. Rafique Umair, K. H., "Dual-band microstrip patch antenna array for 5G mobile communications," *2017 Progress In Electromagnetics Research Symposium — Fall (PIERS — FALL)*, 55–59, Singapore, Nov. 19–22, 2017.
12. Amin, M. M., M. Mansor, N. Misran, and M. Islam, "28/38 GHz dual band slotted patch antenna with proximity-coupled feed for 5G communication," *2017 International Symposium on Antennas and Propagation (ISAP)*, 1–2, 2017.
13. Sunthari, P. M. and R. Veeramani, "Multiband microstrip patch antenna for 5G wireless applications using MIMO techniques," *2017 First International Conference on Recent Advances in Aerospace Engineering (ICRAAE)*, 1–5, 2017.
14. Ali, M. M. M. and A.-R. Sebak, "Design of compact millimeter wave massive MIMO dual-band (28/38 GHz) antenna array for future 5G communication systems," *2016 17th International Symposium on Antenna Technology and Applied Electromagnetics (ANTEM)*, 1–2, 2016.
15. Yan, K., P. Yang, F. Yang, L. Zeng, and S. Huang, "Eight-antenna array in the 5G smartphone for the dual-band MIMO system," *2018 IEEE International Symposium on Antennas and Propagation & USNC/URSI National Radio Science Meeting*, 41–42, 2018.
16. Hasan, M. N. and M. Seo, "Compact omnidirectional 28 GHz 2×2 MIMO antenna array for 5G communications," *2018 International Symposium on Antennas and Propagation (ISAP)*, 1–2, 2018.
17. Hong, W., K.-H. Baek, and S. Ko, "Millimeter-wave 5G antennas for smartphones: Overview and experimental demonstration," *IEEE Transactions on Antennas and Propagation*, Vol. 65, 6250–6261, 2017.
18. Chaudhari, A. A. and R. K. Gupta, "A simple tri-band MIMO antenna using a single ground stub," *Progress In Electromagnetics Research C*, Vol. 86, 191–201, 2018.
19. Balanis, C. A., *Antenna Theory — Analysis and Design*, A John Wiley & Son, Inc., Publication, 2005.
20. Jetti, C. R. and V. R. Nandanavanam, "Compact MIMO antenna with WLAN band-notch characteristics for portable UWB systems," *Progress In Electromagnetics Research C*, Vol. 88, 1–12, 2018.
21. Salamin, M. A., S. Das, and A. Zugari, "Design and realization of low profile dual-wideband monopole antenna incorporating a novel ohm (Ω) shaped DMS and semi-circular DGS for wireless applications," *AEU-International Journal of Electronics and Communications*, Vol. 97, 45–53, 2018.
22. Sharawi, M. S., *Printed MIMO Antenna Engineering*, Artech House, 2014.